

Imaging neural activity in worms, flies and mice with improved GCaMP calcium indicators

Lin Tian¹, S Andrew Hires¹, Tianyi Mao¹, Daniel Huber¹, M Eugenia Chiappe¹, Sreekanth H Chalasani², Leopoldo Petreanu¹, Jasper Akerboom¹, Sean A McKinney^{1,4}, Eric R Schreier³, Cornelia I Bargmann², Vivek Jayaraman¹, Karel Svoboda¹ & Loren L Looger¹

Genetically encoded calcium indicators (GECIs) can be used to image activity in defined neuronal populations. However, current GECIs produce inferior signals compared to synthetic indicators and recording electrodes, precluding detection of low firing rates. We developed a single-wavelength GCaMP2-based GECI (GCaMP3), with increased baseline fluorescence (3-fold), increased dynamic range (3-fold) and higher affinity for calcium (1.3-fold). We detected GCaMP3 fluorescence changes triggered by single action potentials in pyramidal cell dendrites, with signal-to-noise ratio and photostability substantially better than those of GCaMP2, D3cpVenus and TN-XXL. In *Caenorhabditis elegans* chemosensory neurons and the *Drosophila melanogaster* antennal lobe, sensory stimulation-evoked fluorescence responses were significantly enhanced with GCaMP3 (4–6-fold). In somatosensory and motor cortical neurons in the intact mouse, GCaMP3 detected calcium transients with amplitudes linearly dependent on action potential number. Long-term imaging in the motor cortex of behaving mice revealed large fluorescence changes in imaged neurons over months.

Calcium is a universal second messenger regulating essential cellular signaling events in many tissues and organisms. In neurons, action potentials (APs) trigger large and rapid changes in cytoplasmic-free calcium concentration. Similarly, activation of glutamate receptors during synaptic transmission produces $[Ca^{2+}]$ transients in dendritic spines. Calcium imaging using synthetic calcium indicators has been used to measure neuronal spiking and synaptic input across populations of neurons *in vitro*¹ and *in vivo*^{2,3}. However, synthetic indicators are difficult to target to specific cell types or subcellular locations (for an exception, see ref. 4). The loading procedures are invasive and damaging to neural tissue, precluding repeated, chronic *in vivo* measurements.

Genetically encoded calcium indicators (GECIs) (also called fluorescent calcium indicator proteins; FCIPs) are an alternative to synthetic indicators. GECIs can be easily targeted to specific cell types or subcellular compartments (for a review, see ref. 5). They

are compatible with long-term, repeated *in vivo* measurements⁶. GECIs consist of a calcium-binding domain such as calmodulin or troponin C, fused to either one or two fluorescent proteins (for review see refs. 7,8). In single-fluorescent-protein GECIs, the fluorescence intensity of a circularly permuted fluorescent protein (cpFP) is modulated by calcium binding-dependent changes in the chromophore environment^{9,10}. In two-fluorescent-protein GECIs, calcium binding modulates fluorescence resonance energy transfer (FRET) between fluorescent proteins^{11–13}.

GECIs have been iteratively improved and are becoming useful for quantitative imaging of neural activity *in vivo*. The calmodulin-based FRET indicator D3cpVenus (D3cpV)¹³ has recently been reported to detect single APs in pyramidal neurons in organotypic mouse brain slices and *in vivo*¹⁴. The troponin C-based indicator TN-XXL has been used for chronic *in vivo* activity imaging in the mouse brain⁶. Among single fluorescent protein-based GECIs, the GCaMP family has found the broadest use across multiple model organisms^{15–17}. However, the properties of all available GECIs are still inferior to those of synthetic indicators in terms of signal-to-noise ratio (SNR), response linearity, photostability and properly tuned calcium affinity. The GCaMP indicators also suffer from poor protein stability. Improvements in each of these parameters would facilitate imaging of neural activity.

Recently, the Ca^{2+} -bound and Ca^{2+} -free structures of GCaMP2 have been solved^{18,19}, forming the basis for rational improvement of indicator properties. Using a combination of protein structure-guided mutagenesis and semi-rational library screening (for a review of GECI design, see ref. 20), we developed improved GCaMP variants. The best mutant, GCaMP3, is brighter, has greater protein stability and has a larger dynamic range and higher affinity for calcium compared to GCaMP2. GCaMP3 is more photostable than the FRET indicators D3cpV and TN-XXL and had much greater sensitivity and faster kinetics, especially at higher levels of activity. GCaMP3 had improved sensitivity in mammalian cell culture and in pyramidal neurons in brain slices as well as in worms, flies and mice *in vivo*.

¹Howard Hughes Medical Institute, Janelia Farm Research Campus, Ashburn, Virginia, USA. ²Howard Hughes Medical Institute, Laboratory of Neural Circuits and Behavior, The Rockefeller University, New York, New York, USA. ³Department of Chemistry, University of Puerto Rico, Río Piedras, San Juan, Puerto Rico. ⁴Present address: The Stowers Institute, Kansas City, Missouri, USA. Correspondence should be addressed to L.L.L. (loogerl@janelia.hhmi.org).

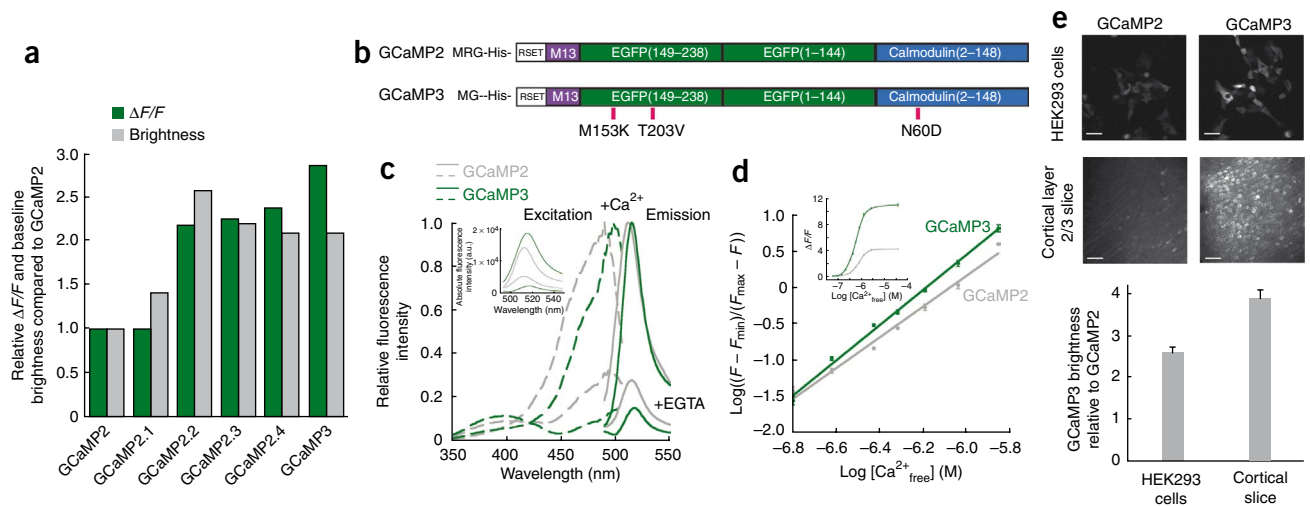


Figure 1 | *In vitro* characterization of GCaMP3. **(a)** Screening resulted in several mutants with improved baseline brightness and signal change in HEK293 cells. **(b)** Schematic representation of GCaMP2 and GCaMP3. Mutated residues are indicated. **(c)** Fluorescence spectra of GCaMP3 and GCaMP2 (1 μ M protein) with 1 mM Ca²⁺ or 10 mM EGTA in MOPS buffer (30 mM MOPS and 100 mM KCl; pH 7.5) (average of three independent measurements). The fluorescence intensity of each indicator was normalized to the peak of the calcium-saturated spectrum. The inset shows the unnormalized fluorescence emission spectra (485-nm excitation). **(d)** Ca²⁺ titration curve (1 μ M protein) in MOPS buffer. Inset, dynamic range of the two indicators. **(e)** Baseline fluorescence of GCaMP3 and GCaMP2. Both indicators were either transfected into HEK293 cells or virally delivered to layer 2/3 cortical neurons. Images were taken either 48 h after transfection or 12 d after viral injection (left), then analyzed with Volocity 5.0 (Improvision) (right). Scale bar, 50 μ m. Error bars indicate s.d. of the mean ($n = 10$).

RESULTS

Structure-guided engineering of GCaMP3

In HEK293 cells, the fluorescence of GCaMP2 was 100-fold lower than that of EGFP (Supplementary Fig. 1a). Addition of a proteasome inhibitor (10 μ M lactacystin) increased the baseline fluorescence of HEK293 cells expressing GCaMP2 (Supplementary Fig. 1b). We reasoned that an N-terminal arginine, found immediately after the initiator methionine of GCaMP2, might destabilize the protein²¹. Indeed, HEK293 cells transfected with a plasmid encoding the mutant lacking the arginine, named GCaMP2.1, showed 40% higher baseline fluorescence than those transfected with GCaMP2 (Supplementary Fig. 1b).

We then created small libraries of GCaMP2.1 variants via site-directed mutagenesis at many sites, both near the EGFP chromophore and at 'superfolder GFP' positions²² (Supplementary Fig. 2). Although screening of GCaMP mutants in bacterial lysate achieved high throughput, we found that the baseline fluorescence and dynamic range correlated only weakly with these properties in more intact preparations (Supplementary Fig. 3). Therefore, we designed a medium-throughput mammalian cell-based assay in HEK293 cells. We induced calcium transients by activating endogenous muscarinic receptors with acetylcholine (Supplementary Fig. 3d). Acetylcholine titrations of GCaMP-transfected HEK293 cells revealed two point mutants with increased dynamic range and baseline fluorescence (T116V, T203V in EGFP; and M66K, M153K in GFP). We named one single mutant (T116V) GCaMP2.2 and a double mutant (T116V and M66K), GCaMP2.3 (Fig. 1a, Supplementary Fig. 4 and Supplementary Table 1).

To increase GCaMP's affinity for calcium to allow better detection of the small and rapid calcium increases associated with individual APs, we analyzed mutations in the EF hand motifs and the interface between the M13 peptide and calmodulin (Supplementary Fig. 2). The amino acid substitution N363D (calmodulin N60D) in both GCaMP2.2 and GCaMP2.3 increased the fluorescence change

for small calcium transients, with little effect on baseline fluorescence (Fig. 1a and Supplementary Fig. 4). GCaMP2.2-N363D and GCaMP2.3-N363D were named GCaMP2.4 and GCaMP3, respectively (Fig. 1a, b and Supplementary Table 1). GCaMP3 had the largest signal change in the acetylcholine assay (Fig. 1a, b and Supplementary Fig. 4), and we further characterized it.

The fluorescence spectra of purified GCaMP3 are similar to those of GCaMP2, with a slight red shift of the excitation maximum (Fig. 1c). GCaMP3 protein assayed in 3-(*N*-morpholino)propane-sulfonic acid (MOPS) buffer had a dynamic range (F_{\max}/F_{\min} ; F_{\max} is fluorescence at saturating [Ca²⁺], and F_{\min} is fluorescence at 0 [Ca²⁺]) of ~12, threefold larger than GCaMP2 (Fig. 1d). This results from a twofold decrease of calcium-free fluorescence and a 1.5-fold increase of calcium-saturated fluorescence (Fig. 1c). The affinity of GCaMP3 for Ca²⁺ was ~1.3-fold higher than that of GCaMP2 (660 ± 19 nM versus 840 ± 25 nM; $P = 0.0017$, paired *t*-test) (Fig. 1d).

In HEK293 cells GCaMP3 showed ~2.6-fold higher baseline fluorescence than GCaMP2 (Fig. 1e). When expressed via viral gene transduction in cortical layer 2/3 neurons, baseline fluorescence was ~3.9-fold higher than that of GCaMP2 (Fig. 1e). Given the lower fluorescence of purified GCaMP3 in the apo state, the increase in baseline fluorescence was likely caused by increased protein expression and stability at 37 °C.

Characterization of GCaMP3 in brain slice

We measured the AP-triggered fluorescence responses^{23,24} of GCaMP3 in pyramidal neurons in cultured brain slices (Fig. 2a, b) and acute neocortical brain slices at room temperature (22–25 °C; Fig. 2c, d). In a cultured slice, the GCaMP3 plasmid was delivered by biolistic transfection. Increases in GCaMP3 fluorescence intensity ($\Delta F/F = 46 \pm 4.2\%$, $n = 9$ cells) at the base of the apical dendrite were detected reliably in response to single APs in all cells (100% single-trial detection; Supplementary Fig. 5a). The average $\Delta F/F$ of GCaMP3 ($n = 9$ cells) was $185 \pm 13\%$, $250 \pm 27\%$, $320 \pm 35\%$, $480 \pm 50\%$,

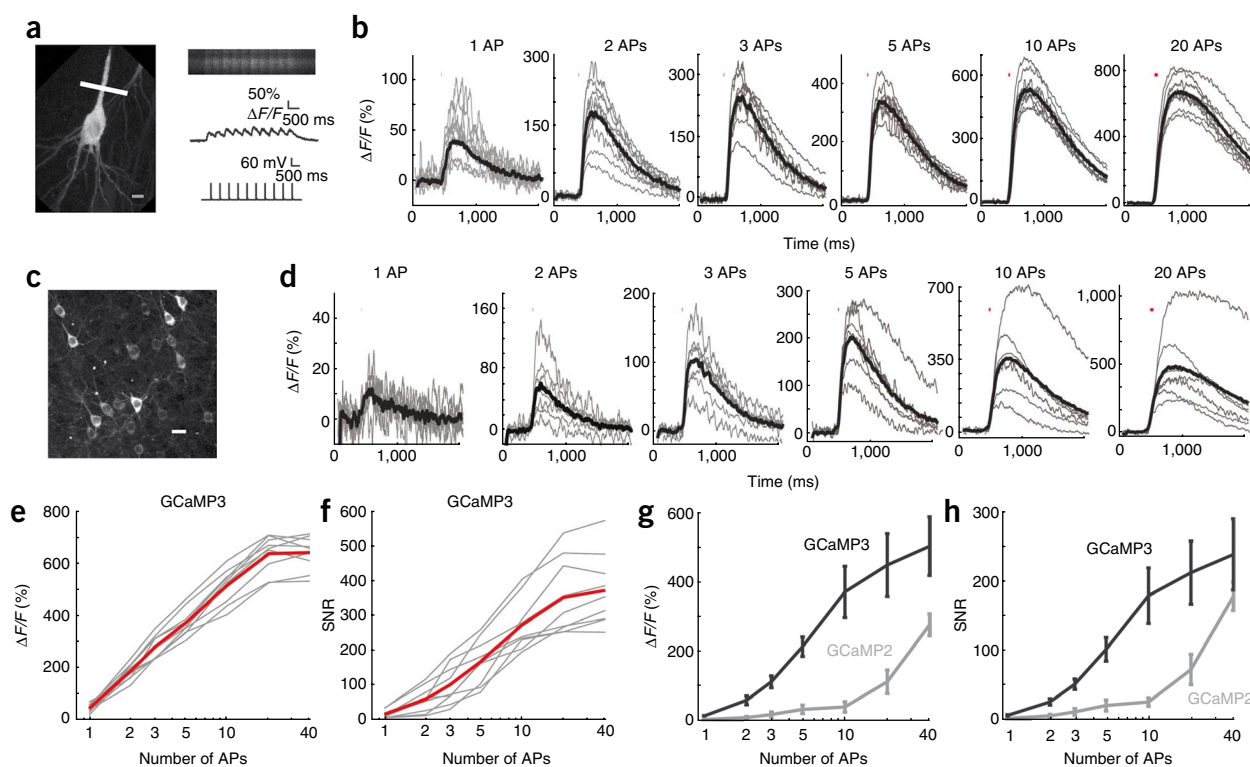


Figure 2 | Action potential-evoked response of GCaMP3 in hippocampal pyramidal and layer 2/3 cortical neurons. **(a)** Fluorescence image showing the linescan location at the base of the apical dendrite and evoked APs in the soma (left). Scale bar, 10 μm . Raw line-scan images showing fluorescence baseline and single AP-evoked responses (right). **(b)** Trial-averaged responses of GCaMP3 for individual hippocampal pyramidal cells in organotypic slices ($n = 9$ cells; gray) and mean across all cells (black) for each stimulus. Note different y-axis scales. **(c)** Expression of GCaMP3 in layer 2/3 cortical neurons (S1) via *in utero* plasmid electroporation. Scale bar, 20 μm . **(d)** Trial-averaged responses of GCaMP3 for individual layer 2/3 cortical cells ($n = 9$ cells, gray) in response to trains of APs given at 83 Hz, and the mean across cells (black). Note different y-axis scales. **(e, f)** Amplitudes and SNR of GCaMP3 responses for individual hippocampal pyramidal cells (gray) in response to trains of APs given at 83 Hz and the mean for all cells (red). **(g, h)** Average response **(g)** and SNR **(h)** of GCaMP3 and GCaMP2. Error bars, s.d. of the mean ($n = 9$).

600 \pm 100% and 620 \pm 130% for 2, 3, 5, 10, 20 and 40 AP, respectively (Fig. 2b,e). The signal-to-noise ratio (SNR; Online Methods) of GCaMP3 was 16.3 \pm 10.9, 167.1 \pm 65.1 and 371.4 \pm 102.8 for 1 AP, 5 APs and 40 APs, respectively (Fig. 2f). The fluorescence increase and single AP detection efficiency were significantly ($P = 0.001$) improved over GCaMP2 (1 AP $\Delta F/F = 17 \pm 10\%$; 38% single-trial detection)²⁴. The kinetics of the GCaMP3 fluorescence response in a cultured hippocampal slice were similar to those of GCaMP2 (GCaMP3: rise half-life ($t_{1/2}$) = 83 \pm 2 ms and decay $t_{1/2}$ = 610 \pm 32 ms; GCaMP2: rise $t_{1/2}$ = 95 \pm 15 ms and decay $t_{1/2}$ = 480 \pm 130 ms²⁴; all measurements for 10-AP stimulus). The improved properties of GCaMP3 allow imaging spontaneous population activities in a cultured hippocampal slice, as opposed to GCaMP2, which produced no discernible signal above background fluorescence (Supplementary Movies 1, 2 and Supplementary Fig. 6).

We next tested the performance of GCaMP3 in layer 2/3 (L2/3) somatosensory cortical pyramidal neurons after long-term expression driven by the CAG promoter via *in utero* electroporation (Fig. 2c and Supplementary Fig. 5b). The average $\Delta F/F$ of GCaMP3 at the base of the apical dendrite was 14 \pm 2.7% ($n = 9$ cells) for single APs and 505 \pm 220% for 40 APs (Fig. 2d,g, Supplementary Fig. 5b and Supplementary Table 2). Compared to $\Delta F/F$ and SNR of GCaMP2 ($n = 8$ cells), these properties of GCaMP3 were 2–5-fold larger (Fig. 2g,h and Supplementary Table 2). Individual APs in single trials could be resolved at rates up to 6 Hz (Supplementary Fig. 7). The threshold for 100% spike detection in acute brain slices

was 2 APs, with a 1 AP detection rate of $\sim 90\%$ (Supplementary Figs. 5b and 8a), slightly inferior to the performance in cultured brain slices. The source of this discrepancy is unknown.

Comparison of GCaMP3 and FRET-based GECIs

We compared the performance of D3cpV and TN-XXL (Fig. 3a) to that of GCaMP3 under identical experimental conditions. At baseline calcium levels, the FRET indicators (based on intact fluorescent proteins) were brighter than GCaMP3 (data not shown). However, the smaller fluorescence changes produced by the FRET indicators (Fig. 3b,c, Supplementary Fig. 9 and Supplementary Table 2) resulted in lower SNR compared to GCaMP3 (Fig. 3d–f and Supplementary Table 2). Furthermore, GCaMP3 was more photostable than the FRET indicators. After 10 cycles of 150 s of frame-scan illumination of the soma and proximal dendrite (10 mW at the sample), interspersed by 30 s of darkness, GCaMP3 fluorescence remained unchanged (109% of starting fluorescence), whereas TN-XXL (36% CFP; 70% YFP) and D3cpV (59% CFP; 84% YFP) had reduced fluorescence (Fig. 3g). The mean fluorescence rise times were similar: 95 \pm 27 ms, 80 \pm 18 ms and 108 \pm 26 ms for GCaMP3, TN-XXL and D3cpV (Fig. 3h). The fluorescence decay time of GCaMP3 (650 \pm 230 ms, $n = 7$ cells), was significantly shorter than for the FRET indicators (TN-XXL, 1,550 \pm 640 ms, $n = 10$ cells ($P = 0.0016$, paired *t*-test); D3cpV, 9,500 \pm 3,400 ms, $n = 10$ cells ($P = 1.7 \times 10^{-5}$, paired *t*-test)) (Fig. 3h).

In terms of absolute response and SNR, GCaMP3 performed better than both FRET indicators over the entire stimulus range,

Figure 3 | Comparison of GECI responses in pyramidal cell principal dendrite in acute cortical slice to back-propagating APs.

(a) Schematic representation of the FRET-based calcium indicators D3cpV and TN-XXL. M13, M13 peptide. (b) Mean of fluorescence responses for AP trains across cells ($n = 7$ cells, 1 trial each cell). Traces (bottom to top) represent the response to trains of 1, 2, 3, 5, 10, 20 and 40 APs. (c) Ratio change of individual hippocampal pyramidal cells (gray) expressing D3cpVenus ($n = 11$ cells) or TN-XXL ($n = 10$ cells) in response to trains of APs given at 83 Hz and the mean across cells (black). (d) SNR of D3cpV and TN-XXL. (e,f) Comparison of mean responses ($\Delta F/F$ or $\Delta R/R$) and SNR of GCaMP3, D3cpV and TN-XXL. Inset, close-up of lower stimuli. (g) Mean cellular fluorescence during periodic two-photon frame scans (GCaMP3, $n = 4$ cells; TN-XXL, $n = 4$ cells; and D3cpVenus, $n = 3$ cells). (h) Rise and decay time comparison of all three indicators at 10 APs. Error bars, s.d. of the mean (D3cpV, $n = 10$ cells; TN-XXL, $n = 10$ cells; and GCaMP3, $n = 8$ cells (c–f, h)).

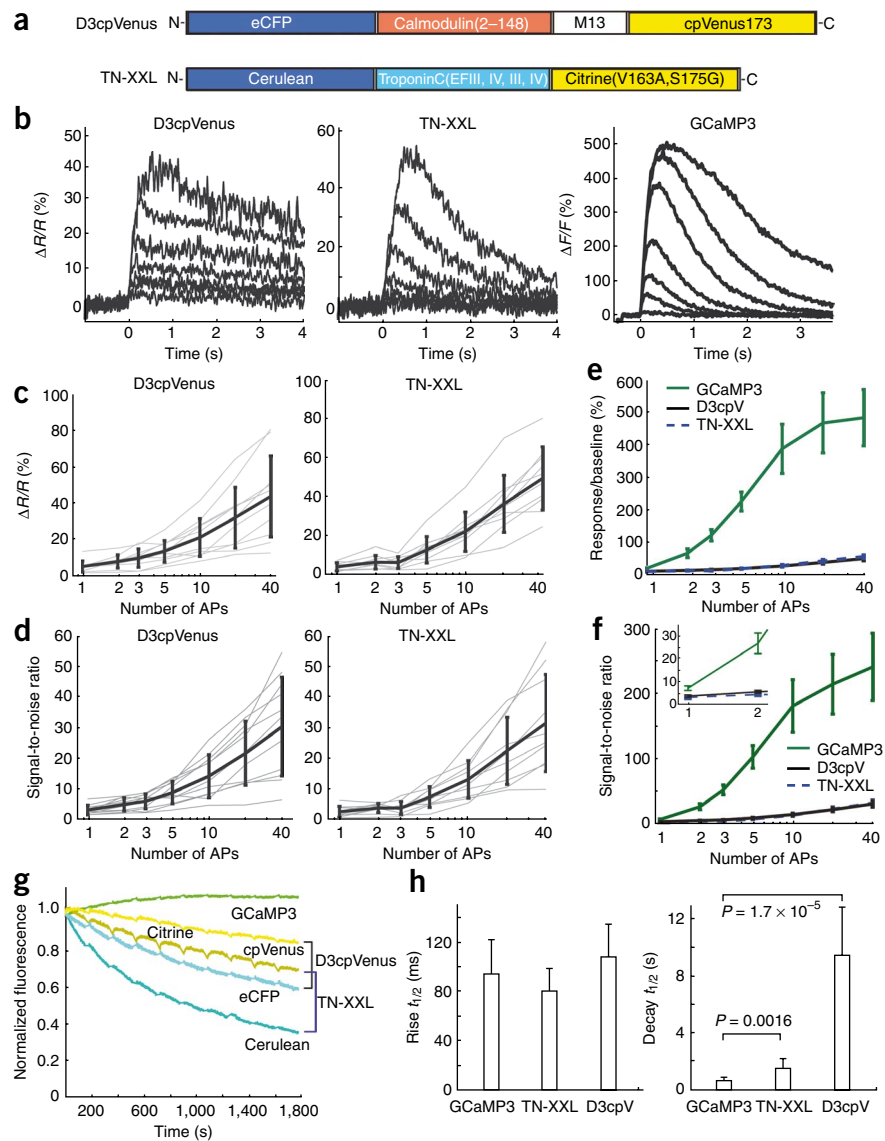
particularly from 2–20 APs (Fig. 3f and Supplementary Table 2). GCaMP3 also showed greater photostability and faster kinetics (Fig. 3g,h). These factors translate into improved detection and measurement of physiologically relevant calcium signals (Supplementary Fig. 8a).

Imaging sensory-evoked Ca^{2+} transients in *C. elegans*

To compare the performance of GCaMP3 with previous GCaMPs in response to sensory stimulation-evoked activity in sensory neurons, we created stable *C. elegans* lines expressing GCaMP1, GCaMP2 and GCaMP3 in one of the two AWC neurons (AWC^{on}). Expression of GCaMP1 and GCaMP2 in AWC neurons caused behavioral perturbations in some of the transgenic lines, reflected by decreased local search turning. In contrast, GCaMP3-expressing worms showed no detectable cytotoxicity or behavioral perturbation (Supplementary Fig. 10 and Supplementary Table 3). We imaged individual worms after an odor addition-removal sequence¹⁶. Presentation of isoamyl alcohol inhibited AWC^{on} , causing a decrease in fluorescence for all three GCaMP indicators (Fig. 4a,b). The fluorescence change was larger for the two newer GCaMPs relative to GCaMP1 ($-13 \pm 6\%$ for GCaMP1, $-27 \pm 8\%$ for GCaMP2, $-38 \pm 8\%$ for GCaMP3). Subsequent removal of the attractive odor resulted in an average of $455 \pm 48\%$ fluorescence increase in AWC^{on} neurons expressing GCaMP3, a ~ 4 – 5 -fold improvement over that of GCaMP2 ($113 \pm 25\%$ $\Delta F/F$) and GCaMP1 ($88 \pm 19\%$ $\Delta F/F$) (Fig. 4c,d). Variation in sensor expression owing to the mosaic nature of transgenesis precluded quantitative comparison of indicator baseline brightness.

Imaging sensory-evoked Ca^{2+} transients in *Drosophila*

We then expressed GCaMP1.6 and GCaMP3 in a broad subset of *Drosophila* olfactory projection neurons in the antennal lobe and compared their responses to odor application (GCaMP2 does



not express well in *Drosophila*²⁵). Single copies of GCaMP were sufficient to produce visible fluorescence (data not shown) in glomeruli of the antennal lobe, but we used two copies to allow imaging at low laser intensities. We imaged neural activity in an identified glomerulus, DM2 (Fig. 5a) in response to the presentation of two odors, vinegar and isoamyl acetate. We found a ~ 4 -fold increased fluorescence change in DM2 for GCaMP3 compared to GCaMP1.6, as measured by frame scans (Fig. 5b,c) in response to vinegar (average $\Delta F/F$ of GCaMP3 is $143.7 \pm 16.7\%$; average $\Delta F/F$ of GCaMP1.6 is $39.3 \pm 10.9\%$). We obtained similar results with glomerulus DM2 when the fly was stimulated with isoamyl acetate odor (data not shown). These data show that GCaMP3 is a major improvement over existing GCaMPs for measuring sensory-evoked Ca^{2+} transients in invertebrates.

Imaging *in vivo* Ca^{2+} transients in mouse cortex

To test GCaMP3 in vertebrates, we delivered it to layer 2/3 somatosensory or motor cortical neurons via infection with adeno-associated virus (AAV2/1; *synapsin-1* promoter). Twelve days after infection, we observed robust expression of GCaMP3 in layer 2/3 pyramidal neurons (Fig. 1e). We used two-photon microscopy to

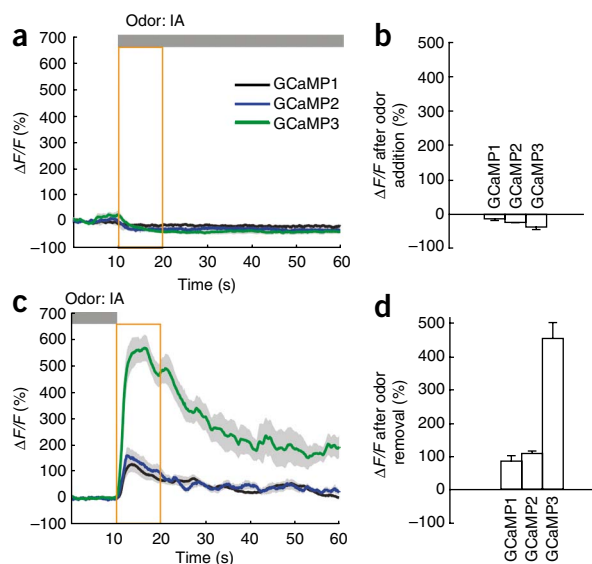


Figure 4 | *In vivo* imaging of sensory-evoked Ca^{2+} transients with GCaMPs in *C. elegans*. (**a–d**) Odor presentation-evoked (**a,b**) and odor removal-evoked (**c,d**) responses of GCaMP1, GCaMP2 and GCaMP3 in *C. elegans* olfactory neurons. Transgenic worm lines expressing GCaMPs were imaged after an odor addition-removal sequence. Gray bars denote odor presence. Data collected during the intervals marked with a yellow box were analyzed in **b** and **d**. Gray shading of each trace and error bars indicate s.e.m. ($n = 12$ worms for each genotype).

physiology in some cells. We observed bright nuclear fluorescence at P25–P28 in ~8.3% of GCaMP3-, 13% of D3cpV- and 5% of TN-XXL-labeled L2/3 pyramidal neurons (**Supplementary Fig. 11a**). Neurons with filled nuclei had attenuated GCaMP fluorescence responses (data not shown), and reduced calcium changes evoked by neural activity (**Supplementary Fig. 11b**). Immunostaining with an antibody to the 6His tag detected predominantly cytosolic GCaMP3, suggesting that the nuclei were filled with N-terminally cleaved GCaMP3 (**Supplementary Fig. 11c**). These results suggest that both calcium homeostasis and GECI function are impaired in neurons with labeled nuclei.

When GCaMP3 was introduced postnatally via viral transduction (under the control of the *synapsin-1* promoter), some neurons near the injection site were bright and had fluorescent nuclei (**Supplementary Fig. 11d**). The spontaneous fluorescence transients of nuclear-filled neurons had long decay times, another signature of abnormal physiology (**Fig. 6f**). These perturbed cells were easily visually identified for exclusion. Basal fluorescence decreased with distance from the injection site and was nucleus-excluded over large areas of the brain, even after 120 d of expression (**Fig. 6f** and **Supplementary Fig. 11d**). We used a variety of physiological methods to test for altered properties of fluorescent neurons (GCaMP3-positive) with nonfluorescent nuclei. We recorded in brain slices from neurons expressing GCaMP3 for 2–3 weeks. GCaMP3-positive neurons had similar resting potential and excitability compared to GCaMP3-negative cells (**Supplementary Fig. 12a,b**). We used laser scanning photostimulation circuit mapping²⁷ to test for changes in synaptic properties of GCaMP3-positive neurons. We found that GCaMP3-positive and GCaMP3-negative neurons had indistinguishable total synaptic input (**Supplementary Fig. 12c,d**). Thus, selection of neurons displaying nuclear-excluded GCaMP3 expression allowed quantitative optical physiology analysis on broad swathes of cortical surface.

As a demonstration of chronic *in vivo* calcium imaging, we used adenovirus-delivered GCaMP3 to image the *in vivo* calcium activity of motor cortical neurons repeatedly through a cranial window (**Fig. 6g**). Many neurons displayed large-amplitude fluorescence transients during a 140 s imaging period while head-fixed mice ran

image labeled cell bodies while simultaneously recording APs in whole-cell or cell-attached configurations (**Fig. 6a**).

We first tested the fluorescence changes of GCaMP3 evoked by APs that were triggered by brief current pulses in anesthetized mice. The average fluorescence response of GCaMP3 was nearly linearly related to the number of APs in trains of 1, 2, 3, 5 or 10 at 50 Hz (**Fig. 6b,c**). A single AP caused a fluorescence increase of $7.9 \pm 2.8\%$ ($n = 9$ cells) (**Fig. 6c**). For bursts of 2, 3, 5 and 10 AP, the corresponding responses were $12.5 \pm 6.4\%$, $21.2 \pm 6.4\%$, $43.7 \pm 18.0\%$ and $94.7 \pm 42.5\%$, respectively ($n = 9$ cells) (**Fig. 6c**). The detection rate was 70% for single pulses, 90% for trains of 3 AP and 100% for longer trains (**Supplementary Fig. 8b**). Consistent with rapid calcium extrusion at physiological temperature (37°C)²⁶, GCaMP3 showed faster kinetics *in vivo* (decay $t_{1/2}$ at 10 pulses: 384 ± 76 ms) compared to slice preparations ($P = 0.0015$, paired t -test).

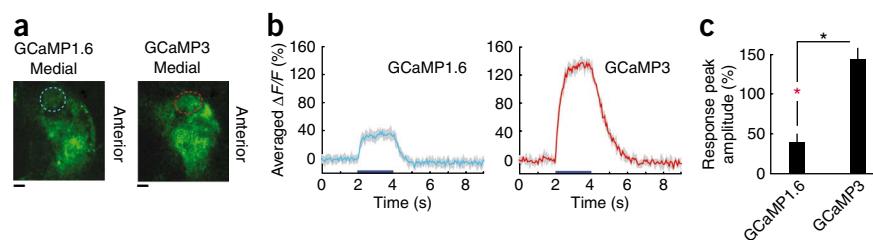
We next imaged the fluorescence changes of GCaMP3 in response to sensory-evoked and spontaneous calcium transients in the primary motor cortex of awake mice running on a treadmill while recording APs in a loose seal cell-attached configuration (**Fig. 6d**). The fluorescence change of GCaMP3 linearly correlated with the number of APs from 3 up to 20 APs per 0.5 s ($n = 6$ cells from three animals) (**Fig. 6e**). Single and double APs were not reliably detected, likely owing to movement noise and elevated baseline calcium levels in the awake brain.

Chronic imaging with GCaMP3 in mice

We found that long-term expression of GECIs in cortical neurons introduced via *in utero* electroporation caused altered

Figure 5 | *In vivo* imaging of sensory-evoked Ca^{2+} transients with GCaMPs in *Drosophila*.

(**a**) Fluorescence images showing odor-evoked responses of GCaMP1.6 and GCaMP3 in DM2 glomeruli (projection neurons) of the *Drosophila* antennal lobe. DM2 region of interest, indicated with a dashed line, was used for frame scans. Scale bars, 10 μm . (**b**) Comparison of DM2 frame-scan responses of GCaMP1.6 and GCaMP3 to addition of vinegar. Five-trial average response of a single fly in each trial, expressing GCaMP1.6 (left) or GCaMP3 (right). (**c**) Peak response of GCaMP1.6 (four antennal lobes from three flies) and GCaMP3 (four antennal lobes from four flies) across all trials and flies. $*P = 6.80 \times 10^{-8}$, Mann-Whitney test. Gray shading and error bars indicate s.d. of the mean ($n = 20$).



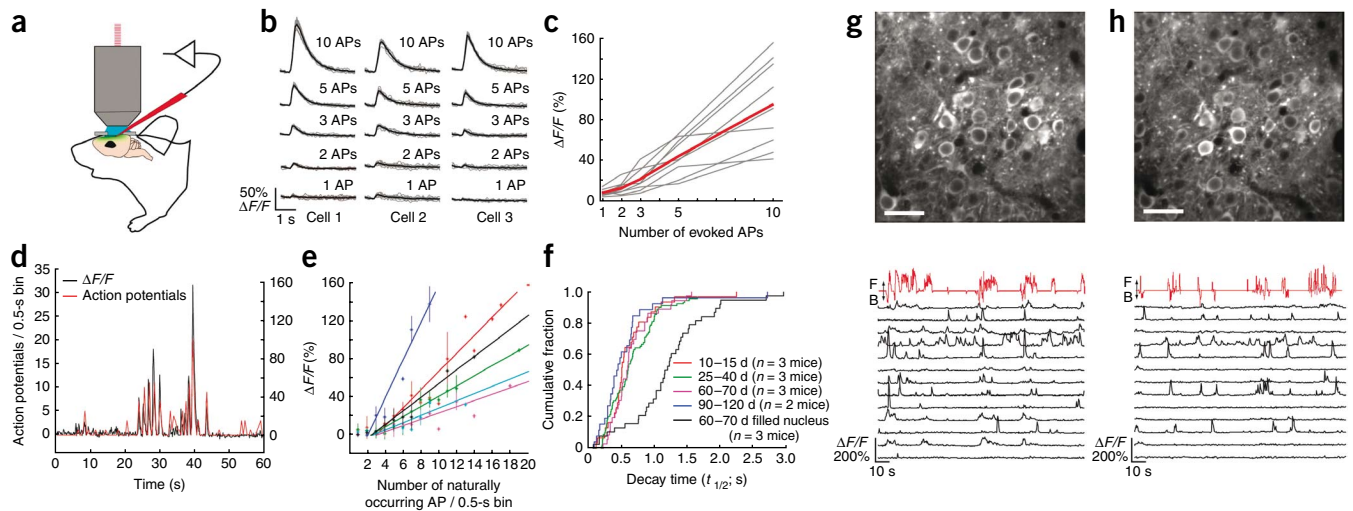


Figure 6 | *In vivo* Ca^{2+} imaging of evoked and spontaneous activity with GCaMP3 in awake, behaving mice. **(a)** Schematic illustrating simultaneous two-photon imaging and electrophysiology in virally infected L2/3 neurons *in vivo*. **(b)** Examples of single-trial responses (gray) and average across 10 trials (black) from three neurons to evoked APs at 50 Hz with mouse under anesthesia. **(c)** GCaMP3 showed linear $\Delta F/F$ in response to evoked APs ($n = 9$ cells, gray; average of 10 trials per neuron, red). **(d)** Example trace of simultaneous recording of fluorescence changes (black) and spiking activity (red, number of APs per 0.5 s bin) during head-fixed behavior. APs were recorded in loose seal cell-attached mode. **(e)** Fluorescence change in response to APs, binned over 0.5 s intervals. Six cells from three mice were indicated with different colors. Error bars, s.d. of the mean. **(f)** Cumulative distribution of the decay times ($t_{1/2}$, single-exponential fit from last fluorescence maximum). Decay times of neurons with nuclear exclusion are similar at 10–120 d (colored lines, $P = 0.22$, Kolmogorov-Smirnov test). Neurons with fluorescent nuclei had significantly longer decay times (black, $P = 5.78 \times 10^{-10}$, Kolmogorov-Smirnov test). **(g)** GCaMP3 expression in L2/3 neurons of the primary motor cortex at 72 d after injection (top; scale bar, 30 μm) and $\Delta F/F$ traces of individual cells (bottom; black lines). Relative treadmill movement indicated by the red line (F: forward, B: backward). **(h)** The same field of view and fluorescent traces as in **g** at 120 d after injection.

on a treadmill²⁸ (Fig. 6g and Supplementary Movie 3). Population activity in the motor cortex was correlated with locomotor activity (Fig. 6g). The fluorescence decay rates of spontaneous calcium transients in imaged cells with nuclear exclusion were stable 120 d after infection (Fig. 6f). Repeated imaging of the same neuronal population at 72 and 120 d after infection showed remarkably constant signal change (Fig. 6h). These results demonstrate that GCaMP3 is suitable for long-term imaging of behaviorally correlated activity in large neuronal populations over extended periods of time.

DISCUSSION

The improved properties of GCaMP3 allow new types of neuroscience applications in multiple model organisms. In *C. elegans*, expression of GECIs has caused behavioral phenotypes²⁹, likely owing to altered neural physiology caused by indicator overexpression. Neurons expressing GCaMP3 showed high SNR without detectable cytotoxicity or behavioral perturbations. The much higher signal levels provided by GCaMP3 may allow experiments with lower expression levels, ameliorating problems associated with calcium buffering.

In *Drosophila*, the poor expression of GCaMP2 (ref. 25) has left GCaMP1.3 and 1.6 as the state-of-the-art single-fluorescent-protein indicators, but their poor sensitivity and nonlinear response has precluded detection of low firing rates³⁰. GCaMP3 showed greatly improved expression and signal levels *in vivo* with no apparent cytotoxicity or behavioral phenotype (data not shown) and could permit imaging experiments not previously possible.

In behaving mice, GCaMP3 allows the simultaneous recording of the activity of dozens of identified neurons over months. Thus, GCaMP3 should allow tracking learning-induced changes in circuit-level activity over multiple recording sessions. Pan-neuronal expression of GCaMP3 might allow widefield

imaging of whole-cortex activity and signal propagation akin to super-resolution functional MRI³¹.

Long-term, high-level expression of GECIs in the mouse brain can result in nonfunctional indicators³² and abnormal physiology. Though expression of GCaMP3 in the postnatal brain, mediated by viral gene transfer, limited such adverse effects, the proportion of neurons with fluorescent nuclei still increased with proximity to the injection site and slowly increased with time after injection. Therefore, optimizing the timing and magnitude of expression to balance signal levels and cytotoxicity needs further study and may require optimization on a case-by-case basis.

Ratiometric indicators have potential advantages over single-fluorescent-protein GECIs, including higher baseline brightness and insensitivity to motion artifacts via wavelength ratioing. However, GCaMP3 is more photostable, likely because of reduced bleaching in the low-fluorescence state. Ratiometric measurements could be achieved with GCaMP3 by co-expression or fusion of a reference fluorescent protein. The smaller size of GCaMP3 potentially facilitates a wider array of targeted protein fusions for calcium imaging in subcellular compartments. The faster kinetics of GCaMP3 may allow more faithful detection of the number and timing of APs in spike trains.

GCaMP3 may not be the most suitable GECI for all applications. Single APs can also be detected using D3cpV¹⁴; indeed, the slow kinetics of D3cpV might be suitable for situations characterized by very low and sparse spike rates. Troponin-based indicators, such as TN-XXL, may cause less perturbation of endogenous calcium signaling⁶. Prudence dictates testing each of these indicators in the context of specific applications.

Although GCaMP3 is a major improvement over GCaMP2, additional avenues for protein engineering remain. Mutagenesis

to ablate interactions of the calmodulin and M13 peptide domains of GCaMP, such as that done to the D2/D3/D4 indicators¹³, may improve performance at high expression levels. A single-fluorescent-protein indicator based on troponin C³³ might combine the benefits of a nonendogenous calcium-binding protein with the high signal-to-noise and fast kinetics of GCaMP. Quantitative modeling studies²⁰ have suggested that increasing the fluorescence on-rate would further improve detection of the brief calcium transients associated with single APs. Expression cassettes that maintain steady, moderate levels of GCaMP3 expression for months would facilitate signal calibration and reduce toxicity concerns.

METHODS

Methods and any associated references are available in the online version of the paper at <http://www.nature.com/naturemethods/>.

Note: Supplementary information is available on the Nature Methods website.

ACKNOWLEDGMENTS

We thank J. Simpson and S. Hampel for cloning GCaMPs into pMUH, and members of the Fly Core for making fly crosses. pMUH was a generous gift from B. Pfeiffer and G. Rubin. We thank J. Seelig, who contributed to the *Drosophila* imaging experiments, S. Viswanathan and S. Sternson for assistance in screening mutants in HEK293 cells, J. Marvin for assistance in screening mutants in *Escherichia coli*, B. Zemelman for assistance in virus production, H. Zhong, T. Sato and B. Borghuis for developing image analysis software, D.K. O'Connor for assistance with *in utero* electroporation, H. White and S. Winfrey for cell culture, B. Shields and A. Hu for immunostaining, A. Arnold for helping with imaging experiments, members of the Molecular Biology Shared Resource for plasmid preparation and sequencing, and J. Marvin, J. Simpson and G. Tervo for critical reading of the manuscript. All affiliations are Howard Hughes Medical Institute, Janelia Farm Research Campus. GCaMP2 plasmid was a gift from M. Kotlikoff (Cornell University); TN-XXL plasmid was a gift from O. Griesbeck (Max Planck Institute of Neurobiology); D3cpVenus plasmid was a gift from A. Palmer (University of Colorado); GH146-Gal4 flies were a gift from L. Luo (Stanford University); UAS-GCaMP1.6 flies were a gift from D. Rieff and A. Borst (Max Planck Institute of Neurobiology).

AUTHOR CONTRIBUTIONS

L.L.L., K.S., L.T., S.A.H. and T.M. designed the project; L.T. and L.L.L. designed the sensor and screen in *E. coli* and HEK293 cells; L.T., T.M., S.A.H. and L.P. tested the GCaMP variant in brain slice; S.A.H. tested FRET sensor and GCaMP2 in brain slice; S.A.H., L.T. and D.H. analyzed imaging data of brain slice and *in vivo*; D.H. performed *in vivo* mouse brain imaging; S.H.C. and C.I.B. performed worm imaging and data analysis; V.J. and M.E.C. performed calcium imaging and data analysis in the fly; S.A.M. and S.A.H. analyzed data for AP detection probability; J.A., L.L.L. and E.R.S. analyzed the structure; L.L.L. and L.T. led the project; L.L.L., K.S., L.T. and S.A.H. wrote the paper.

Published online at <http://www.nature.com/naturemethods/>.

Reprints and permissions information is available online at <http://npg.nature.com/reprintsandpermissions/>.

1. Yuste, R., Peinado, A. & Katz, L.C. Neuronal domains in developing neocortex. *Science* **257**, 665–669 (1992).
2. Stosiek, C., Garaschuk, O., Holthoff, K. & Konnerth, A. *In vivo* two-photon calcium imaging of neuronal networks. *Proc. Natl. Acad. Sci. USA* **100**, 7319–7324 (2003).
3. Fetcho, J.R., Cox, K.J. & O'Malley, D.M. Monitoring activity in neuronal populations with single-cell resolution in a behaving vertebrate. *Histochem. J.* **30**, 153–167 (1998).
4. Tour, O. *et al.* Calcium Green FAsH as a genetically targeted small-molecule calcium indicator. *Nat. Chem. Biol.* **3**, 423–431 (2007).
5. Palmer, A.E. & Tsien, R.Y. Measuring calcium signaling using genetically targetable fluorescent indicators. *Nat. Protocols* **1**, 1057–1065 (2006).

6. Mank, M. *et al.* A genetically encoded calcium indicator for chronic *in vivo* two-photon imaging. *Nat. Methods* **5**, 805–811 (2008).
7. McCombs, J.E. & Palmer, A.E. Measuring calcium dynamics in living cells with genetically encodable calcium indicators. *Methods* **46**, 152–159 (2008).
8. Mank, M. & Griesbeck, O. Genetically encoded calcium indicators. *Chem. Rev.* **108**, 1550–1564 (2008).
9. Baird, G.S., Zacharias, D.A. & Tsien, R.Y. Circular permutation and receptor insertion within green fluorescent proteins. *Proc. Natl. Acad. Sci. USA* **96**, 11241–11246 (1999).
10. Nagai, T., Sawano, A., Park, E.S. & Miyawaki, A. Circularly permuted green fluorescent proteins engineered to sense Ca²⁺. *Proc. Natl. Acad. Sci. USA* **98**, 3197–3202 (2001).
11. Miyawaki, A. *et al.* Fluorescent indicators for Ca²⁺ based on green fluorescent proteins and calmodulin. *Nature* **388**, 882–887 (1997).
12. Heim, N. & Griesbeck, O. Genetically encoded indicators of cellular calcium dynamics based on troponin C and green fluorescent protein. *J. Biol. Chem.* **279**, 14280–14286 (2004).
13. Palmer, A.E. *et al.* Ca²⁺ indicators based on computationally redesigned calmodulin-peptide pairs. *Chem. Biol.* **13**, 521–530 (2006).
14. Wallace, D.J. *et al.* Single-spike detection *in vitro* and *in vivo* with a genetic Ca²⁺ sensor. *Nat. Methods* **5**, 797–804 (2008).
15. He, J., Ma, L., Kim, S., Nakai, J. & Yu, C.R. Encoding gender and individual information in the mouse vomeronasal organ. *Science* **320**, 535–538 (2008).
16. Chalasani, S.H. *et al.* Dissecting a circuit for olfactory behaviour in *Caenorhabditis elegans*. *Nature* **450**, 63–70 (2007).
17. Wang, J.W., Wong, A.M., Flores, J., Vosshall, L.B. & Axel, R. Two-photon calcium imaging reveals an odor-evoked map of activity in the fly brain. *Cell* **112**, 271–282 (2003).
18. Akerboom, J. *et al.* Crystal structures of the GCaMP calcium sensor reveal the mechanism of fluorescence signal change and aid rational design. *J. Biol. Chem.* **284**, 6455–6464 (2008).
19. Wang, Q., Shui, B., Kotlikoff, M.I. & Sondermann, H. Structural basis for calcium sensing by GCaMP2. *Structure* **16**, 1817–1827 (2008).
20. Hires, S.A., Tian, L. & Looger, L.L. Reporting neural activity with genetically encoded calcium indicators. *Brain Cell Biol.* **36**, 69–86 (2008).
21. Varshavsky, A. The N-end rule at atomic resolution. *Nat. Struct. Mol. Biol.* **15**, 1238–1240 (2008).
22. Pedelacq, J.D., Cabantous, S., Tran, T., Terwilliger, T.C. & Waldo, G.S. Engineering and characterization of a superfolder green fluorescent protein. *Nat. Biotechnol.* **24**, 79–88 (2006).
23. Pologruto, T.A., Yasuda, R. & Svoboda, K. Monitoring neural activity and [Ca²⁺] with genetically encoded Ca²⁺ indicators. *J. Neurosci.* **24**, 9572–9579 (2004).
24. Mao, T., O'Connor, D.H., Scheuss, V., Nakai, J. & Svoboda, K. Characterization and subcellular targeting of GCaMP-type genetically encoded calcium indicators. *PLoS ONE* **3**, e1796 (2008).
25. Hendel, T. *et al.* Fluorescence changes of genetic calcium indicators and OGB-1 correlated with neural activity and calcium *in vivo* and *in vitro*. *J. Neurosci.* **28**, 7399–7411 (2008).
26. Markram, H., Helm, P.J. & Sakmann, B. Dendritic calcium transients evoked by single back-propagating action potentials in rat neocortical pyramidal neurons. *J. Physiol. (Lond.)* **485**, 1–20 (1995).
27. Shepherd, G.M. & Svoboda, K. Laminar and columnar organization of ascending excitatory projections to layer 2/3 pyramidal neurons in rat barrel cortex. *J. Neurosci.* **25**, 5670–5679 (2005).
28. Dombeck, D.A., Khabbazi, A.N., Collman, F., Adelman, T.L. & Tank, D.W. Imaging large-scale neural activity with cellular resolution in awake, mobile mice. *Neuron* **56**, 43–57 (2007).
29. Ferkey, D.M. *et al.* *C. elegans* G protein regulator RGS-3 controls sensitivity to sensory stimuli. *Neuron* **53**, 39–52 (2007).
30. Jayaraman, V. & Laurent, G. Evaluating a genetically encoded optical sensor of neural activity using electrophysiology in intact adult fruit flies. *Front Neural Circuits* **1**, 3 (2007).
31. Kim, S.G. & Ogawa, S. Insights into new techniques for high resolution functional MRI. *Curr. Opin. Neurobiol.* **12**, 607–615 (2002).
32. Hasan, M.T. *et al.* Functional fluorescent Ca²⁺ indicator proteins in transgenic mice under TET control. *PLoS Biol.* **2**, e163 (2004).
33. Garaschuk, O., Griesbeck, O. & Konnerth, A. Troponin C-based biosensors: a new family of genetically encoded indicators for *in vivo* calcium imaging in the nervous system. *Cell Calcium* **42**, 351–361 (2007).



ONLINE METHODS

Construct and virus production. The original GCaMP2 expression construct was obtained from M. Kotlikoff³⁴, TN-XXL from O. Griesbeck⁶ and D3cpV from A. Palmer¹³. Genes encoding GCaMPs were subcloned into pRSETa for expression and purification in *E. coli*. Genes encoding GCaMPs were subcloned into pCMV for HEK293 cell assays and cultured brain slice experiments. Genes encoding GCaMP variants, TN-XXL and D3cpV were subcloned into the pCAGGS vector with a CAG promoter (CMV enhancer, β -actin promoter and regulatory element from the woodchuck hepatitis virus³⁵ (WPRE)) for *in utero* electroporation³⁶. pCAG-mCherry³⁷ was transfected along with GCaMP plasmids for cultured hippocampal slices and *in utero* electroporation for better control of expression. To make transgenic worms and flies, GCaMPs were subcloned into pSM under control of the *str-2* promoter and pMUH (a gift from B. Pfeiffer, Janelia Farm Research Campus), respectively. pMUH-GCaMPs were incorporated into an attP40 integrase site on the second *Drosophila* chromosome³⁸ (Genetic Services, Inc.). For *in vivo* calcium imaging in mice, GCaMP2 and GCaMP3 were expressed using an adeno-associated virus 2/1 (AAV2/1) driving the sensor under control of the pan-neuronal human *synapsin-1* promoter³⁹. GCaMP2 and GCaMP3 were subcloned into the rAAV-hSYN expression vector, and live virus was produced (University of Pennsylvania Vector Core Services). All constructs were verified by sequencing.

Bacterial protein expression, purification and testing. Genes encoding GCaMPs in pRSETa were transformed into chemically competent BL21(DE3)-pLysS and purified via the N-terminal histidine tag. Protein concentration was determined by intrinsic tryptophan fluorescence. Calcium clamping was performed at pH 7.2 with 10 mM blends of K_2H_2EGTA and Ca_2EGTA from the Calcium Calibration Kit 1 (Invitrogen). Free $[Ca^{2+}]$ levels were calculated using Maxchelator. Fluorescence spectra were recorded on a Safire² fluorescence plate reader (Tecan). The dynamic range here is calculated as F_{max}/F_{min} . F_{max} is the fluorescence intensity at saturating $[Ca^{2+}]$ and F_{min} is the fluorescence intensity at zero $[Ca^{2+}]$.

HEK293 cell-based screen. Genes encoding GCaMPs in pCMV were transfected into HEK293 cells using Lipofectamine 2000 (Invitrogen), and imaging experiments were performed 48 h after transfection. HEK293 cells transfected with GCaMPs in 96-well plate were imaged on an FDSS plate reader (Hamamatsu). Acetylcholine was automatically added 10 s after read initiation. Brightness was quantified using Volocity 5.0 (Improvision).

Calcium imaging in worms. Calcium imaging of GCaMP-expressing worms was performed as described previously¹⁶. A total of 12 worms for each genotype were studied in a custom-designed microfluidic device, and the fluorescence response to odor stimulation was averaged. For odor presentation, each animal was first starved in the imaging chip for 20 min. Odors were presented at $t = 10$ s in a 60-s recording, and removed 5 min later, at $t = 10$ s in a second 60-s recording.

Mouse brain slice preparation. Hippocampal slice cultures were prepared using standard methods^{24,40}. For biolistic gene transfer, 10 μ g of DNA was used per full tube. Imaging experiments

were performed 24–48 h after biolistic transfection. For acute slice experiments, GECIs were introduced into gestational day 16 (E16) mouse embryos by *in utero* electroporation³⁵, and acute slices were prepared at P14–P17 as described before²⁴.

Fly stocks, preparation and odor delivery. Flies were reared on standard cornmeal agar medium. We used the Gal4-UAS system⁴¹ to direct the expression of the calcium sensors to projection neurons. *GH146-Gal4* flies were a gift from L. Luo (Stanford University). *UAS-GCaMP1.6* flies were a gift from D. Reiff and A. Borst (Max Planck Institute of Neurobiology, Martinsried). All experimental animals were adult females, 3–5 d after eclosion. Adult flies were dissected using previously described methods¹¹. Flies were anesthetized in a vial on ice just until movement stopped (~15 s) and then gently inserted into a hole in a piece of aluminum foil. Small drops of wax (55 °C) were used to suspend the fly in the hole, with the edge of foil defining a horizontal plane around the head and thorax, from the first antennal segment anteriorly to the scutellum posteriorly. The dorsal side of the foil was bathed in saline, while the ventral side (including antennae and maxillary palps) remained dry and accessible to odors. A window was cut in the dorsal head cuticle between the eyes, extending from the ocelli to the first antennal segment. Fat and air sacs dorsal and anterior to the brain were removed, but the perineural sheath was left intact. The proboscis was affixed with a small drop of wax to a strand of human hair to limit brain movement. Spontaneous leg movements were typically observed in this preparation for the duration of the recording (1.5–3 h). The saline composition used in all experiments was⁴²: 103 mM NaCl, 3 mM KCl, 5 mM *N*-tris(hydroxymethyl) methyl-2-aminoethanesulfonic acid, 10 mM trehalose, 10 mM glucose, 2 mM sucrose, 26 mM $NaHCO_3$, 1 mM NaH_2PO_4 , 1.5 mM $CaCl_2$ and 4 mM $MgCl_2$, adjusted to 275 mOsm, pH 7.3 when bubbled with 95% O_2 and 5% CO_2 .

Odors (*cis*-3-hexen-1-ol and isoamyl acetate) were delivered using a custom-made odor-delivery system and a Teflon nozzle (entry diameter 1/8 inch) directed toward the antennae. Odors were delivered in a constant stream of air (1 liter min^{-1}) at final concentrations of about 15%. Odor delivery times were measured using a mini-photoionization detector (Aurora Scientific Inc.). Odors were presented for either 3 s or 5 s. All comparisons of sensor performance were made using experiments with identical odor presentation times. The results reported are based on data obtained from three GCaMP1.6-expressing flies (four antennal lobes) and four GCaMP3-expressing flies (four antennal lobes).

Calcium imaging in fly. We imaged on a two-photon laser-scanning microscope (Prairie Technologies) using an Olympus 0.8 NA LUMPIFI40XW/IR2 objective. A mode-locked Ti:Sapphire Chameleon Ultra II laser (Coherent) tuned to 920 nm was used as excitation source. Fluorescence was collected using photomultiplier tubes (Hamamatsu) after bandpass filtering using a 525/70 nm emission filter. Images were acquired using Prairie View software in frame-scan mode (4–16 Hz) for a single plane of one antennal lobe.

Electrophysiology and calcium imaging in brain slice. We made recordings from CA1 cells in hippocampal slice culture, and cortical layer 2/3 pyramidal cells (S1) in acute brain slices at

room temperature (22–24 °C). Patch pipettes were pulled from borosilicate glass (standard wall with filament) and had 4–6 M Ω resistance when filled with internal solution (128 mM potassium methylsulfate or potassium gluconate, 10 mM HEPES, 10 mM sodium phosphocreatine, 4 mM MgCl₂, 4 mM Na₂ATP, 0.4 mM Na₂GTP, 3 mM ascorbic acid (pH 7.25, 290 mOsm)). Slice recording and simultaneous line-scan imaging were performed as before²⁴. During recording, slices were bathed in ACSF (127 mM NaCl, 25 mM NaHCO₃, 1.25 mM NaH₂PO₄, 25 mM glucose, 2.5 mM KCl, 2 mM CaCl₂ and 1 mM MgCl₂) bubbled with carbogen. Cells were selected for data analysis if they had nuclear exclusion of GECI fluorescence, input resistances of at least 100 M Ω , and resting potentials \leq -50 mV in cultured slice, or \leq -65 mV in acute slice. For experiments with evoked-AP stimuli, 10 μ M (R)-CPP (Tocris) and 10 μ M NBQX (Sigma) were added to the bath to block glutamate receptors. APs were triggered at 83 Hz by current injection (1–4 nA, 2 ms) through the patch pipette.

Imaging was performed in line-scan mode (500 Hz) across the apical dendrite, 20–50 μ m from the base (Fig. 2a). The Ti:Sapphire laser (Mai Tai, Spectro-Physics) was tuned to 910 nm for GCaMPs imaging and 860 nm to excite FRET indicators. For GCaMPs expressed with mCherry, we separated fluorescence into green and red channels with a 565 nm dichroic, and BG22 (green channel) and HQ620/90 (red channel) emission filters. For the FRET-based GECIs, we separated fluorescence with a 505 nm dichroic and HQ480/80 (cyan channel) and HQ535/50 (yellow channel) emission filters. The PMT dark current was subtracted from all traces. In slice culture recordings, mean baseline fluorescence (F_0) was calculated from the filter raw trace (20 Hz) before the AP stimuli, as in ref. 24. Peak fluorescence was determined by averaging 30 ms of the raw fluorescence time series about the peak of the trace linearly filtered at 20 Hz. For acute slices, response baseline was defined as the mean of the 250 ms window immediately before stimulation. Peak response was calculated as the maximum value of the filtered trace (100 ms moving window) within 500 ms of stimulation cessation. This method gave \sim 3% $\Delta F/F$ for 0 AP traces. Noise was calculated on a per-cell level, as the mean s.d. of stimulation-free, 1 second, bleach-corrected trace segments. For display, example traces were filtered with a Savitzky-Golay filter (second order, 50-ms span). AP detection was quantified both by a double-blind psychometric test and by algorithmic template matching. In the psychometric test, eight volunteers were shown a response template and asked if it was present in randomly ordered, sequentially presented traces. False positive rate was determined by the response to 0 AP traces. The algorithmic method computed the maximum cross-correlation between a template and the fluorescence trace lagged 200 ms about the stimulus onset. Detection success was defined as a cross-correlation value greater than 95% of baseline traces. The baseline trace set consisted of all recorded 0 AP traces plus those traces reversed and/or inverted. The template was the first 1.5 s of the mean 3 AP response (GCaMP3) or the mean 5 AP response (D3cpV, TN-XXL). Rise $T_{1/2}$ of hippocampal neurons was measured as the time between the onset of current injection and the half-peak response. Decay $t_{1/2}$ was measured as the time of half decay of a single exponential fit of the recovery from peak response to baseline. All analysis was performed with MATLAB (Mathworks).

In vivo calcium imaging and electrophysiology in mice. rAAVs (AAV2/1; *synapsin-1* promoter) were injected into the primary somatosensory cortex (S1) of 2–3-week-old C57Bl/6Crl wild-type mice. Two weeks after injection, mice were anesthetized with 2% isoflurane, and a 1.5 mm circular craniotomy was performed over the injection site as previously described⁴³. Cells were recorded with a patch pipette containing: 10.0 mM KCl, 140 mM potassium gluconate, 10 mM HEPES, 2.0 mM MgCl₂, 2.0 mM CaCl₂, 0.05 mM Alexa Fluor 594, pH 7.25 and 290 mOsm. For recording and stimulation a MultiClamp 700B amplifier (Molecular Devices) was used. In whole cell mode, APs were evoked by 2–5 ms long current injections; in cell-attached mode currents up to 100 nA were necessary. The Ti:sapphire laser (Mai Tai, Spectro-Physics) was tuned to 910 nm for GCaMP3 imaging. Fluorescence images were simultaneously acquired using a custom-built, two-photon laser-scanning microscope equipped with a \times 40, 0.8 NA objective (Olympus). Frame scans were acquired at 15 Hz (256 \times 32 pixels) for a period of 3 s.

For imaging awake, head-fixed running mice, virus injection and surgery were identical to the anesthetized condition, except that the injection and craniotomy were performed over the primary whisker and forelimb motor area (M1). In addition, local (Marcaïne) and general (Buprenorphine, 0.1 mg kg⁻¹ IP and ketoprofen, 5 mg kg⁻¹ SC) anesthetics were administered. After full recovery on a heating pad the animals were head restrained but allowed to run freely on a linear treadmill. APs were recorded using a loose-seal cell-attached configuration with patch pipettes filled with buffer (125 mM NaCl, 2.5 mM KCl, 25 mM glucose, 10 mM HEPES, 2 mM CaCl₂, 2 mM MgSO₄, 0.05 mM Alexa Fluor 594 (pH 7.4, 285 mOsm)), and signals were amplified using a MultiClamp 700B (Molecular Devices). To confirm the identity of recorded neurons, each recording was terminated by breaking into the cell and filling with red pipette solution. During the imaging sessions the animals were kept alert by sporadic acoustic stimuli (clapping) or by presenting a pole or mild air puffs to the whisker field. Images were acquired at frame rates of 4–8 Hz at a resolution of 256 \times 512 pixels using a \times 16, 0.8 NA water immersion objective (Nikon USA). All images acquired while awake were corrected for movement artifacts using the ImageJ plug-in TurboReg (<http://bigwww.epfl.ch/thevenaz/turboreg/>). $\Delta F/F$ was calculated by subtracting the baseline fluorescence level (F_0 , 35th percentile of total fluorescence) from the actual fluorescence level and normalized to F_0 .

Chronic calcium imaging in behaving mice. For chronic imaging, surgery and craniotomy were carried out as described above, but the GCaMP3-AAV was injected into the cortex directly before sealing the imaging window with dental acrylic. Chronic imaging was performed on C57BL/6Crl wild-type (infected with AAV2/1-*hsyn1*-GCaMP3) and PV-CRE mice⁴⁴ (infected with CRE-dependent AAV2/1-*hsyn1*-GCaMP3) over periods from 10 to 120 d after infection. To keep the animals alert and active during imaging sessions, mice were water restricted and trained to lick for water rewards upon whisker deflection. Decay times ($\tau_{1/2}$, time at half maximum) were calculated by fitting to a single exponential. All data analysis was performed with MATLAB (Mathworks).

Imaging data analysis. For *in vivo* imaging in worms, fluorescence signals in the AWC cell body were analyzed using automated tracking software and MATLAB scripts as described¹⁶.

In flies, fluorescence time series were then obtained by averaging across the spatial extent of the glomerulus in the frame. In all cases fluorescence changes were calculated relative to baseline fluorescence levels as determined by averaging over 2 s just before odor presentation.

For imaging data analysis in mice *in vivo*, the cell body without nucleus was used as ROI for fluorescent transient analysis. Recordings with spontaneous spikes were excluded. $\Delta F/F$ was the peak fluorescence increase within 500 ms of stimulus onset divided by the mean of the three frames preceding stimulus onset. AP detection was quantified using cross-correlation template-matching with the first six frames of the mean response to 3 APs as a template and the second half of 1 AP and 2 AP traces (1.5–2.83 s after stimulus, 100 total traces) as the baseline. In awake behaving mice, the $\Delta F/F$ of spontaneous fluorescence transients was calculated as the peak fluorescence increase divided by the mean of the 5th–10th percentile of fluorescent intensities. All data analysis was performed with Matlab (MathWorks).

Characterizing intrinsic and circuit properties of GCaMP3 expressing neurons. L2/3 progenitor cells were transfected via *in utero* electroporation in C57BL/6Crl pregnant mice at E16 with a plasmid expressing CRE recombinase under the CAGS promoter as previously described^{36,45}. At postnatal day 14 (P14), a CRE-dependent AAV virus expressing GCaMP3 under the human *synapsin-1* promoter was injected into the neocortex. This combinatorial method allowed us to label a sparse subpopulation of L2/3 pyramidal neurons with GCaMP3. Cells were recorded at a depth of 50 to 95 μm . Immediately after breaking in, cells were depolarized by injection of graded current pulses. We anesthetized the animals 14–21 d after the viral infection (P28–P34), with an intraperitoneal injection of a ketamine and xylazine mixture (0.13 mg ketamine and 0.01 mg xylazine per g body weight) and perfused through the heart with a small volume of ice-cold ACSF containing: 130 mM NaCl, 25 mM NaHCO₃, 25 mM D-glucose, 2.5 mM KCl, 1 mM MgCl₂, 2 mM CaCl₂ and 1.25 NaH₂PO₄, aerated with 95% O₂ 5% CO₂. The brain was removed and placed in an ice-cold cutting solution containing: 110 mM choline chloride, 25 mM NaHCO₃, 25 mM D-glucose, 11.6 mM sodium ascorbate, 7.0 mM MgCl₂, 3.1 mM sodium pyruvate, 2.5 mM KCl, 1.25 mM NaH₂PO₄ and 0.5 mM CaCl₂. We cut 400- μm -thick coronal slices of the barrel cortex with a vibrating slicer (Microm) and incubated in oxygenated ACSF for 45 min at 37 °C before the recordings. Pairs of L2/3 pyramidal neurons (within <100 μm ; one GCaMP3-positive, the other GCaMP3⁻) were recorded sequentially. We compared the synaptic input impinging onto GCaMP3-positive and GCaMP3-negative neurons by measuring the total excitatory input onto both recorded cells

using laser-scanning photostimulation by glutamate uncaging. Briefly, stimulation was with an ultraviolet laser (DPSS Lasers) on a grid (16 \times 16, spacing 75 μm). This area included the entire thickness of the cortical gray matter and adjacent barrel columns. MNI-glutamate was uncaged for 1 ms with 20 mW of laser power at the specimen plane. We verified that under our experimental conditions these stimulation parameters elicited APs only when the laser beam was close to the soma of the neurons. Only excitatory inputs were mapped as cells were held at -70 mV, close to the reversal for fast inhibition. Responses were analyzed within 100 ms after the UV-light stimulus. Direct and synaptic responses were separated according to their different onset time³. Responses with an onset time below 7 ms were categorized as direct (that is, purely postsynaptic) and later responses as synaptic. Synaptic input maps were calculated as the mean current in a response window from 7 to 75 ms.

Signal-to-noise ratio (SNR) calculation. SNR was calculated as the ratio of $\Delta F/F$ or $\Delta R/R$ to s.d. of the filtered trace (100-ms moving window), 250 ms before the stimulus up to stimulus onset.

Statistical analysis. *P* values were computed by a Mann-Whitney algorithm in Matlab. All value ranges are given as mean \pm s.d., unless otherwise noted.

34. Kotlikoff, M.I. Genetically encoded Ca²⁺ indicators: using genetics and molecular design to understand complex physiology. *J. Physiol. (Lond.)* **578**, 55–67 (2007).
35. Gray, N.W., Weimer, R.M., Bureau, I. & Svoboda, K. Rapid redistribution of synaptic PSD-95 in the neocortex *in vivo*. *PLoS Biol.* **4**, e370 (2006).
36. Saito, T. & Nakatsuji, N. Efficient gene transfer into the embryonic mouse brain using *in vivo* electroporation. *Dev. Biol.* **240**, 237–246 (2001).
37. Shaner, N.C. *et al.* Improved monomeric red, orange and yellow fluorescent proteins derived from *Discosoma sp.* red fluorescent protein. *Nat. Biotechnol.* **22**, 1567–1572 (2004).
38. Markstein, M., Pitsouli, C., Villalta, C., Celniker, S.E. & Perrimon, N. Exploiting position effects and the gypsy retrovirus insulator to engineer precisely expressed transgenes. *Nat. Genet.* **40**, 476–483 (2008).
39. Thiel, G., Greengard, P. & Sudhof, T.C. Characterization of tissue-specific transcription by the human synapsin I gene promoter. *Proc. Natl. Acad. Sci. USA* **88**, 3431–3435 (1991).
40. Stoppini, L., Buchs, P.A. & Muller, D. A simple method for organotypic cultures of nervous tissue. *J. Neurosci. Methods* **37**, 173–182 (1991).
41. Brand, A.H., Manoukian, A.S. & Perrimon, N. Ectopic expression in *Drosophila*. *Methods Cell Biol.* **44**, 635–654 (1994).
42. Wilson, R.I. & Laurent, G. Role of GABAergic inhibition in shaping odor-evoked spatiotemporal patterns in the *Drosophila* antennal lobe. *J. Neurosci.* **25**, 9069–9079 (2005).
43. Huber, D. *et al.* Sparse optical microstimulation in barrel cortex drives learned behaviour in freely moving mice. *Nature* **451**, 61–64 (2008).
44. Hippenmeyer, S. *et al.* A developmental switch in the response of DRG neurons to ETS transcription factor signaling. *PLoS Biol.* **3**, e159 (2005).
45. Petreanu, L., Huber, D., Sobczyk, A. & Svoboda, K. Channelrhodopsin-2-assisted circuit mapping of long-range callosal projections. *Nat. Neurosci.* **10**, 663–668 (2007).